

Interstellar Seeing. II. The Case of the Vela Pulsar: Source Unresolved

J. M. Cordes

Astronomy Department and NAIC, Cornell University, Ithaca, NY 14853
cordes@spacenet.tn.cornell.edu

submitted to *Astrophysical Journal* November 28, 2018

ABSTRACT

I use a method based on interstellar scintillations for discerning information about source sizes on scales less than one micro-arc sec. I use a comprehensive model for a pulsar signal, scintillated amplitude modulated noise, that includes source fluctuations and noise statistics. The method takes into account time-frequency averaging in the signal processing as well as effects due to source structure. The method is applied to interferometric visibility data on the Vela pulsar which show slightly less scintillation modulation than expected for a point source in the strong scattering regime. The decreased scintillation modulation is likely to be due exclusively to time-frequency averaging rather than from any source size effects. The implied upper limit on source extent, derived through Bayesian inference, is compared to predictions that take into account beaming from the relativistic plasma flow in neutron star magnetospheres. The upper limit for the transverse source size ($\lesssim 400$ km at 95% confidence for a pulsar distance of 0.5 kpc) is easily consistent with conventional models for radio emission regions in pulsar magnetospheres that place them well inside the light cylinder at only a few neutron-star radii from the star's surface.

1. Introduction

Diffraction interstellar scintillation (DISS) is caused by multipath scattering of radio waves from small-scale irregularities in the ionized interstellar medium. In a previous paper (Cordes 2000; hereafter paper I) methodologies have been presented that exploit DISS as a superresolution phenomenon: one that can constrain or determine source sizes on scales that are orders of magnitude smaller than the inherent diffraction resolution of the largest apertures available, those involving space VLBI. In this paper we use some of the methods of Paper I to assess recent results reported on the Vela pulsar (Gwinn *et al.* 1997, 2000; hereafter G97 and G00, respectively), including the conclusion that the magnetosphere of that pulsar has been resolved.

G97 analyzed VLBI observations of the Vela pulsar using time and frequency resolutions that exploit the spatial resolving power of DISS. Through estimation of the probability density function (PDF) of the visibility function magnitude, they infer that DISS shows less modulation

than expected from a point source and therefore conclude that the source must be extended. They estimate a transverse size ~ 500 km for the region responsible for the pulsed flux in a narrow range of pulse phase.

We reconsider the observations of G97 because effects other than source size can diminish the modulation index (the rms fractional modulation) from the unity value expected for a point source in the strong scattering regime (see Rickett 1990 and Cordes & Lazio 1991 for definitions of this regime). In particular, even modest averaging in time and in frequency over a narrow bandwidth — a feature of essentially all observations of DISS — can reduce the modulation index to below unity. We show explicitly that the averaging parameters used by G97 can account for the entire reduction of the modulation index. To interpret their data, we adopt a Bayesian method to place limits on the source size.

G00 presented another analysis of data on Vela that took into account some aspects of time-frequency averaging and other effects that can alter the visibility PDF. They revise downward the estimate of source size to ~ 440 km. Our treatment in this paper contests this result also. However, the biggest uncertainty in establishing a detection of or limit on source size is in the DISS parameters, the scintillation bandwidth and time scale. We discuss the role of the uncertainties in these quantities in some detail.

In §2 we summarize relevant observations of the Vela pulsar and in §3 we outline the use of DISS to resolve sources, including a discussion of isoplanatic scales and formulae for the second moment and the PDF of measured interferometer visibilities. In §4 we apply a Bayesian inference method to data on the Vela pulsar which yields an upper bound on the source size. §5 discusses the anticipated scale sizes of pulsar emission regions and interprets our upper limit on Vela pulsar. The paper is summarized in §6. Much of the paper refers to Paper I.

2. Observations of the Vela Pulsar

The Vela pulsar is ideal for DISS studies that aim at resolving its magnetosphere because it is very bright and, as shown below, the DISS isoplanatic scale is smaller than the magnetosphere of the pulsar. G97 report visibility measurements on the Vela pulsar made at a frequency ~ 2.5 GHz. They show that the scattering diameter of this strongly scattered pulsar is slightly elongated, with dimensions (FWHM) of $3.3 \pm 0.2 \times 2.0 \pm 0.1$ mas. They also report values for the DISS time scale and bandwidth of $\Delta t_d \approx 15$ s and $\Delta \nu_d \approx 39 \pm 7$ kHz, respectively. By comparing the angular diameter with that predicted from the DISS parameters for specific geometries, they conclude that scattering occurs in a thin scattering screen approximately 27% of the total pulsar-earth distance from the pulsar, i.e. $D_s/d = 0.27$, where D_s is the pulsar-screen distance and d is the pulsar-Earth distance. The angular size, DISS bandwidth, and the inferred ratio D_s/d differ significantly from those reported by Desai *et al.* (1992) (1.6 ± 0.2 mas, 68 ± 5 kHz, and 0.81, respectively). The DISS bandwidth measured by G97 agrees, however, with that reported by Cordes (1986) when

scaled to 2.5 GHz using a ν^4 scaling law. More recently, G00 quote different values for the DISS parameters at ~ 2.5 GHz, $\Delta t_d \approx 26 \pm 1$ s and $\Delta \nu_d \approx 66 \pm 1$ kHz. The exact values of the DISS parameters have a strong influence on the visibility fluctuations and on any inference from those fluctuations on source size.

Some DISS observations on the Vela pulsar (Cordes, Weisberg & Boriakoff 1985; Johnston *et al.* 1998; Backer 1974) have suggested that the DISS bandwidth scales very nearly as ν^4 , somewhat different from the $\nu^{22/5}$ scaling commonly associated with the Kolmogorov wavenumber spectrum (Rickett 1990). However, a composite of all available data from the literature, shown in Figure 1, suggests otherwise. Simple, unweighted least-squares fits of log-log quantities yields $\Delta \nu_d \propto \nu^{4.30 \pm 0.12}$, closer to the Kolmogorov scaling than to the ν^4 scaling. The increase in value of the exponent is due largely to the new high frequency measurements by Johnston *et al.* 1998. It is conceivable that there is not a single exponent value for the entire range of frequencies plotted, but the errors do not allow any break point to be established. Similarly, the DISS time scale varies as $\Delta t_d \propto \nu^{1.17 \pm 0.06}$, very close to the $\nu^{6/5}$ Kolmogorov scaling. Residuals from the fits imply that there are typically 9% errors on Δt_d and 22% errors on $\Delta \nu_d$. We use these errors in our inference on source size rather than using the errors quoted by G00. We think the latter are underestimated.

As shown in Paper I and also as calculated by G97, the isoplanatic scale at the pulsar’s location can be calculated from the measured DISS parameters and scattering diameter. The length scale ℓ_d in the diffraction pattern in the observer’s plane is related to the measured angular diameter θ_{FWHM} (assuming a circular, Gaussian brightness distribution and a thin screen) and to the DISS bandwidth as (c.f. Cordes & Rickett 1998, §3.)

$$\ell_d = \frac{\lambda \sqrt{2 \ln 2}}{\pi \theta_{\text{FWHM}}} = \left[\left(\frac{cd \Delta \nu_d}{2\pi \nu^2 C_1} \right) \left(\frac{d}{D_s} - 1 \right) \right]^{1/2}, \quad (1)$$

where $C_1 = 0.957$ for a thin screen with a Kolmogorov spectrum while $C_1 = 1$ for a thin screen with a square-law structure function. Using a nominal value for θ_{FWHM} , 2.6 mas, taken to be the geometric mean of the angular diameters measured by Gwinn *et al.*, we obtain $\ell_d \approx 10^{3.6}$ km. Solving for D_s/d using nominal values for θ_{FWHM} , the DISS bandwidth (from G97), and the distance $d = 0.5$ kpc, we obtain $D_s/d \approx 0.27$, in agreement with G97. We note, however, that the true distance to the pulsar is not well known. Recent work (Cha, Sembach & Danks 1999) suggests that d may be as small as 0.25 kpc, based on association of the pulsar with the Vela supernova remnant. This would yield $D_s/d \approx 0.15$. If we use the DISS bandwidth from G00, however, we get $D_s/d \approx 0.39$ for $d = 0.5$ kpc and $D_s/d \approx 0.24$ using the smaller distance.

In Paper I, we define the isoplanatic scale at the pulsar, $\delta r_{s,iso}$, as the separation that two sources would have if their scintillations are correlated at a level of e^{-1} . This scale is related to the diffraction scale ℓ_d as

$$\delta r_{s,iso} = \frac{(D_s/d)\ell_d}{1 - D_s/d}. \quad (2)$$

Note that the expression is not valid for $D_s \rightarrow d$ because the small-angle approximation employed

in all of our analysis breaks down. Using DISS parameters from G97, the isoplanatic scale $\delta r_{s,iso} \approx 10^{3.1}$ km for $d = 0.5$ kpc and $\delta r_{s,iso} \approx 10^{2.8}$ km for half the distance, $d = 0.25$ kpc. Using G00 parameters, we get $\delta r_{s,iso} = 10^{3.4}$ and $10^{3.1}$ km for the two distances. For comparison, the light cylinder radius is $r_{LC} = cP/2\pi \approx 10^{3.6}$ km (where the spin period is $P = 0.089$ sec), which is larger than the isoplanatic scale by a factor of 3 to 7. Figure 2 shows schematically the pulsar geometry and its relationship to the isoplanatic scale. We discuss the geometry further in §5 below. Later in the paper, we place an upper limit on the source size by choosing the largest of all estimates for the isoplanatic scale, $\delta r_{s,iso} = 10^{3.4}$ km. This gives the least restrictive upper bound.

G97 present a histogram of visibility magnitudes on a baseline that does not resolve the scattering disk. The visibilities were calculated using time-bandwidth averaging intervals of $T = 10$ s and $B = 25$ kHz that resolve the DISS. They integrated over a pulse phase window of 1.16 ms, corresponding to $\Delta t/P = 0.013$ cycles. They also summed over $N_p = 112$ pulse periods to yield their quoted integration time of 10 sec.

The reported histogram departs from the shape expected for a scintillating point source, which Gwinn *et al.* interpret as a signature for source extension, with source size $\approx 460 \pm 110$ km. This result is based on the larger distance estimate for the pulsar (0.5 kpc). The quoted error is said to arise from uncertainty in the scintillation bandwidth, $\Delta\nu_d$.

G97 did not consider the effects of the time-bandwidth averaging on their results. Though T and B are respectively smaller than the nominal DISS time scale and bandwidth, Δt_d and $\Delta\nu_d$, they are large enough to be important in any consideration of visibility fluctuations. In fact, we show that TB averaging can account for *all* the departure of the fluctuations from those expected for a point source. In our analysis below, we also consider contributions to visibility fluctuations from intrinsic variations in the pulsar. We discuss these in some detail in Paper I (Appendix A), where we present the scintillated, amplitude-modulated noise model. Amplitude fluctuations include the well-known pulse-to-pulse variations that typically represent 100% modulations of the pulsed flux at a fixed pulse phase.

G00 presented a new analysis of VLBI data on the Vela pulsar and considered TB averaging on their results. Also, their re-estimated scintillation parameters reduce the role of TB averaging from what it would have been using the G97 estimates so that their inferred source size is much the same as in G97. We argue that this new analysis is incorrect, though the DISS parameters are closer to those extrapolated from other measurements.

3. Resolving Sources with DISS

In Paper I we discuss quantitatively how measurements of interferometric visibilities (or single-aperture intensities) contain information about the intrinsic source size, even for sources unresolved by the interferometer baseline. The issue is whether the source is extended enough to reduce the scintillation modulation. Our discussion is based on the strong-scattering regime,

which easily applies to observations of the Vela pulsar. A number of methods may be used to extract source-size information, including an investigation of the modulation index of the visibility and, more accurately, the full probability density function (PDF) of the visibility magnitude. For pulsars with multiple pulse components (and presumably multiple emission regions), cross-correlation analyses may also be conducted.

3.1. Second Moments & Isoplanatic Scales

To evaluate visibility statistics, we need the autocovariance (ACV) function γ_G of the ‘gain’ G by which the intensity or visibility is modulated by DISS. The gain has unit mean, $\langle G \rangle = 1$. In the strong scattering (Rayleigh) limit the ACV for a spatial offset $\delta \mathbf{r}_s$ at the source, a temporal offset τ and an interferometer baseline b is

$$\gamma_G(\mathbf{b}, \tau, \delta \nu, \delta \mathbf{r}_s) = \langle G(\mathbf{r}, t, \nu, \mathbf{r}_s) G(\mathbf{r} + \mathbf{b}, t + \tau, \nu + \delta \nu, \mathbf{r}_s + \delta \mathbf{r}_s) \rangle - 1 = |\gamma_g(\mathbf{r}, t, \nu, \mathbf{r}_s)|^2. \quad (3)$$

The rightmost equality uses the second moment,

$$\gamma_g(\mathbf{b}, \tau, \delta \nu, \delta \mathbf{r}_s) = \langle g(\mathbf{r}, t, \nu, \mathbf{r}_s) g(\mathbf{r} + \mathbf{b}, t + \tau, \nu + \delta \nu, \mathbf{r}_s + \delta \mathbf{r}_s) \rangle, \quad (4)$$

where g is the wave propagator defined in Paper I. For zero frequency lag γ_g is related to the phase structure function D_ϕ by the well-known relation (e.g. Rickett 1990),

$$\gamma_g(\mathbf{b}, \tau, \delta \nu = 0, \delta \mathbf{r}_s) = e^{-D_\phi(\mathbf{b}, \tau, \delta \mathbf{r}_s)}. \quad (5)$$

In Paper I we give a general expression for D_ϕ that applies to any distribution of scattering material along the line of sight. For the Vela pulsar, scattering evidently is dominated by a thin screen along the line of sight (Desai *et al.* 1992). For a thin screen at distance D_s from the pulsar, we have (Paper I and references therein)

$$D_\phi(\mathbf{b}, \tau, \delta \mathbf{r}_s) \propto \left(\frac{|\mathbf{b}_{\text{eff}}(s)|}{b_e} \right)^\alpha \quad (6)$$

$$\mathbf{b}_{\text{eff}}(\mathbf{b}, \tau, \delta \mathbf{r}_s) = (D_s/d)\mathbf{b} + \mathbf{V}_{\text{eff}}\tau + (1 - D_s/d)\delta \mathbf{r}_s \quad (7)$$

$$\mathbf{V}_{\text{eff}} = (D_s/d)\mathbf{V}_{\text{obs}} + (1 - D_s/d)\mathbf{V}_p - \mathbf{V}_m(D_s), \quad (8)$$

where b_e is the characteristic length scale at which $D_\phi = 1 \text{ rad}^2$. A square-law structure function with $\alpha = 2$ may apply to the Vela pulsar’s line of sight, as discussed in §2, though the bulk of the evidence suggests that α is close to the Kolmogorov value of $5/3$. In Eq. 8 \mathbf{V}_p is the pulsar velocity, \mathbf{V}_{obs} is the observer’s velocity and \mathbf{V}_m is the velocity of the scattering material in the ISM. Note that the offset between sources, $\delta \mathbf{r}_s$, may be smaller or larger than the spatial offset associated with the pulsar velocity, $\mathbf{V}_p\tau$.

Isoplanatic scales are defined using $\gamma_G = e^{-1}$, implying $D_\phi = 1$ and $|\mathbf{b}_{\text{eff}}| = b_e$. The length scale for the diffraction pattern (at the observer’s location) is given by $D_\phi(\ell_d, 0, 0) = 1$ while the isoplanatic scale at the source is given by $D_\phi(0, 0, \delta r_{s,iso}) = 1$. Solving for ℓ_d and $\delta r_{s,iso}$ and eliminating b_e yields Eq. 2.

3.2. Modulation Index

The modulation index of the visibility magnitude, defined as the rms value divided by the mean intensity, has four terms (c.f. Paper I): three associated with the scintillating source intensity and a fourth due to noise, from sky backgrounds and receiver noise, that adds to the wavefield. Here we are concerned with the leading term that is caused by DISS, m_{ISS}^2 . For sources with brightness distribution $I_s(\mathbf{r}_s)$, $m_{\text{ISS}}^2(\mathbf{b}, \tau)$ is given by

$$m_{\text{ISS}}^2(\mathbf{b}, \bar{\tau}) = \langle I \rangle^{-2} \int \int d\mathbf{r}_{s1} d\mathbf{r}_{s2} I_s(\mathbf{r}_{s1}) I_s(\mathbf{r}_{s2}) Q_{\text{ISS}}(\mathbf{b}, \bar{\tau}, \mathbf{r}_{s2} - \mathbf{r}_{s1}, T, B), \quad (9)$$

where averaging over a time span T and bandwidth B is contained in

$$Q_{\text{ISS}}(\mathbf{b}, \bar{\tau}, \delta\mathbf{r}_s, T, B) = (TB)^{-1} \int_{-T}^{+T} d\tau' \left(1 - \left|\frac{\tau'}{T}\right|\right) \int_{-B}^{+B} d\delta\nu \left(1 - \left|\frac{\delta\nu}{B}\right|\right) \times e^{-ikd^{-1}\mathbf{b}\cdot\delta\mathbf{r}_s} \gamma_G(0, \tau' + \bar{\tau}, \delta\nu, \delta\mathbf{r}_s). \quad (10)$$

In these expressions, $\bar{\tau}$ is the time lag that might be imposed in any data analysis where the visibilities from one site are lagged with respect to another. It is easy to show that $Q_{\text{ISS}} \leq 1$, with equality only when $T \rightarrow 0$, $B \rightarrow 0$, and $\delta\mathbf{r}_s = 0$.

Inspection of Eq. 10 shows that visibility fluctuations are independent of baseline \mathbf{b} for unresolved sources, for which the complex exponential $\rightarrow 1$. The baseline-independent property for visibility fluctuations is similar to the conclusion found by Goodman & Narayan (1989). In general, the integrand factor γ_G in Eq. 9-10 is not factorable. Practical cases, such as media with square-law phase structure functions and Kolmogorov media (Paper I), do not show factorability of γ_G . Therefore, the effects of T-B averaging and source size must be considered simultaneously.

Additional contributions to the total modulation index from intrinsic source fluctuations and from additive noise are secondary to our discussion here. They are significant, however, in any practical application where the time-bandwidth product is low and where intrinsic source fluctuations are high. For pulsars, pulse-to-pulse amplitude variations are important when only a few pulses are included in any averaging. Appendices B and C of Paper I gives full expressions for all contributions to intensity variations.

3.3. Number of Degrees of Freedom in Fluctuations

As Eq. 9-10 indicate, TB averaging and extended structure represent integrals over γ_G that diminish scintillation fluctuations. The modulation index of the averaged intensity or visibility depends on time averaging and source extension in similar ways because both increase the number of degrees of freedom in the integrated intensity. The number of degrees of freedom is

$$N_{\text{dof}} = 2m_{\text{ISS}}^{-2} = 2N_{\text{ISS}} \geq 2, \quad (11)$$

where N_{ISS} is the number of independent DISS fluctuations (“scintles”) that are averaged. For observations in the speckle regime, where scintles are resolved in time and frequency, we expect $1 \leq N_{\text{ISS}} \lesssim 2$.

If $m_{\text{ISS}}^2 = 1$ (within errors), the source is unresolved by the DISS, the baseline \mathbf{b} has not resolved the scattering disk, *and* the scintillations cannot have decorrelated over the averaging intervals T and B . The DISS gain G then has an exponential PDF associated with the two degrees of freedom in the scattered wavefield.

Alternatively, $m_{\text{ISS}}^2 < 1$ can signify (1) variation of the DISS over the averaging time or averaging bandwidth; *or* that (2) the source has been resolved by the DISS, i.e. that it is comparable to or larger than the isoplanatic scale of the DISS. To discriminate between these possibilities, auxiliary information is needed that characterizes the dependence of γ_g on its four arguments, \mathbf{b} , τ , $\delta\nu$, and $\delta\mathbf{r}_s$. Such information is obtained by making DISS and angular broadening measurements over a wide range of frequencies (e.g. Rickett 1990). As discussed in §2, evidence suggests that a Kolmogorov medium distributed in a thin screen is relevant.

Complications in estimating m_{ISS}^2 arise from the fact that scintillating sources fluctuate, on inverse-bandwidth time scales and on a variety of longer time scales, and there is additive noise in any real-world receiver system. We consider all such complications in Paper I (main text and Appendices B and C).

3.4. PDF of Visibility Fluctuations

The full histogram of visibility fluctuations is potentially much more sensitive to source structure than is the second moment, as suggested by Gwinn *et al.* (1997, 1998). Here we summarize our derivation in Paper I of the PDF that takes into account intrinsic source fluctuations, which are important for pulsars.

We assume that the interferometer baseline \mathbf{b}_{ij} resolves neither the source nor the scattering disk. Then the time-average visibility can be written as

$$\bar{\Gamma} \approx G\langle I \rangle + \langle \mathcal{N}_i \rangle \delta_{ij} + X + C, \quad (12)$$

where $\langle I \rangle$ is the mean source intensity, δ_{ij} is the Kronecker delta, $\langle \mathcal{N}_i \rangle$ is the mean background noise intensity, X is a real Gaussian random variable (RV) with zero mean, and C is a complex Gaussian RV with zero mean. Source fluctuations are described by X which includes the noise fluctuations and amplitude fluctuations in the amplitude modulated noise model (c.f. Appendix C of Paper I). C includes additive radiometer noise combined with source noise fluctuations, but is uninfluenced by source amplitude fluctuations. Expressions for σ_X^2 and σ_C^2 are given in Appendix C of Paper I.

The PDF for the visibility magnitude is calculated by successively integrating over the PDFs

for the different, independent terms in Eq. 12, as done in Appendix C of Paper I. The PDF for the scaled visibility magnitude, $\gamma = |\bar{\Gamma}|/\sigma_C$, is

$$f_\gamma(\gamma) = \int dG f_G(G) \int dX f_X(X) \left[\gamma e^{-\frac{1}{2}(\gamma^2 + G^2 i^2)} I_0(\gamma i) \right]_{i=(\langle I \rangle + X/G)/\sigma_C} \quad (13)$$

where I_0 is the modified Bessel function. The integrand factor in square brackets is the Rice-Nakagami PDF of a signal phasor added to complex noise (e.g. Thompson, Moran & Swenson 1991, p. 260). In the absence of any source, the PDF is simply $f_\gamma(\gamma) = \gamma e^{-\gamma^2/2}$.

3.4.1. Pulsar Noise Contributions

In Paper I we give detailed examples of the dependence of the visibility PDF on signal to noise ratio and on the X and C terms. In that paper, Eq. C20 gives the PDF of the complex visibility and Eq. C25 gives the PDF of the magnitude of the visibility. Our form for the visibility PDF differs significantly from the equivalent expression in Eq. 11 of G97. The main differences are that (1) we have unequal variances of the real and imaginary parts of $\bar{\Gamma}$; (2) there is a superfluous factor of 2π in Eq. 11 of G97; and (3) the definition of the variances of the real and imaginary parts in G97 is a factor of two too large.

G97 argue that a pulsar’s contributions to visibility fluctuations become unimportant for large averaging times. While the pulsar fluctuations certainly decrease with increased averaging, it is also true for the additive radiometer noise, which contributes to the C term in Eq. 12. Thus, if one is ignored, both should be ignored. However, neither should be ignored, as the shape of the PDF depends on both. In fact, the ratio of pulsar and radiometer contributions is independent of the averaging time and depends only on the system signal to noise ratio, $\langle I \rangle / \langle \mathcal{N}_i \rangle$. In practice, it takes a very strong source for the X term and portions of the C term to be significant. The Vela pulsar is marginally strong enough for this to be the case. We find that the PDF shape is altered by pulsar fluctuations at the level of about 1% at a radio frequency of 2.5 GHz for the Vela pulsar (c.f. Figure 11 of Paper I).

3.4.2. Sensitivity of the PDF to Time-Bandwidth Averaging

As pointed out by G97 and G00, the mode of the visibility PDF is very sensitive to the number of degrees of freedom in the DISS fluctuations. To model the shape of the PDF correctly, N_{ISS} must be correct; but the level of noise fluctuations and the source intensity must also be correct. In paper I we demonstrate how the PDF varies with the number of ISS degrees of freedom, $2N_{\text{ISS}}$. Increases in N_{ISS} can be due to time-frequency averaging or source extent or both. Statistically, the result is the same. A pure point source can have statistics that mimic those given by an extended source if there is sufficient TB averaging. Another effect is that if the channel bandwidth B is varied, N_{ISS} is changed but so too is the signal to noise ratio. Decreasing

the bandwidth reduces N_{ISS} but increases σ_X and σ_C relative to the $G\langle I \rangle$ term in Eq. 12, thus masking source-size effects that might also contribute to the PDF shape. In addition, the PDF shape is sensitive to the nature of the scattering medium (thin screen vs. extended medium, Kolmogorov vs. square-law structure function). For reasons discussed in §2, we adopt a thin screen, Kolmogorov scattering medium. However, we also consider a thin screen with a square-law structure function.

4. Bayesian Analysis of Source Size for the Vela Pulsar

We represent a set of visibility magnitudes as $\{|\bar{\Gamma}|_i, i = 1, N\}$, where the bar denotes that each measurement has been averaged explicitly over time and implicitly over frequency. Given a model for the source and parameters for the scintillations, the likelihood function for the measurements is (using $|\bar{\Gamma}| \equiv \gamma\sigma_C$)

$$\mathcal{L} = \prod_i f_\gamma(\gamma_i)/\sigma_C. \quad (14)$$

Following a Bayesian scheme presented in Paper I, we can infer the posterior PDF for source model parameters Θ ,

$$f_\Theta(\Theta) = \frac{\mathcal{L}}{\int d\Theta \mathcal{L}}, \quad (15)$$

where we have assumed a flat prior for the model parameters (see Paper I).

To proceed, we assume that the only source parameter is the spatial scale σ_r of a circular Gaussian brightness distribution,

$$I_s(\mathbf{r}_s) = I_{s0} \left(2\pi\sigma_r^2\right)^{-1} \exp\left(-\frac{|\mathbf{r}_s|^2}{2\sigma_r^2}\right). \quad (16)$$

We use this distribution to calculate the modulation index (squared) using Eq. 9 for $\mathbf{b} \approx 0, \bar{\tau} \approx 0$ and using appropriate values for $T, B, \Delta t_d$ and $\Delta\nu_d$ (c.f. §2). This yields m_{ISS}^2 as a function of σ_r from which we calculate the number of ISS fluctuations, N_{ISS} , using Eq. 11. For Kolmogorov media, we have used tabulated values of the covariance function from Lambert & Rickett (1999). This, in turn, we use to calculate the PDF for the DISS gain, G , that is used in Eq. 13 to calculate f_γ . Finally, we calculate $f_{\bar{\Gamma}}$ by appropriate scaling of f_γ .

To apply our method, we use the histogram presented in Figure 2 of G97, which we write as $N_k = N f_{\bar{\Gamma}}(\bar{\Gamma}_k)$, $k = 1, N_{\text{bins}}$, where N is the total number of visibility measurements and N_{bins} is the number of bins in the histogram. Using the histogram, we rewrite the likelihood function as a product over bins,

$$\mathcal{L} = \prod_k [f_\gamma(\gamma_k)/\sigma_C]^{N_k}. \quad (17)$$

To calculate the PDF for a given source size, we need the parameters $\text{SNR} \equiv I_{s0}/\sqrt{2}\sigma_+$ (the signal to noise ratio), σ_+ (the rms noise σ_C when there is no source signal), and the number of ISS fluctuations summed in each measurement, $N_{\text{ISS}} = N_{\text{ISS}}(T/\Delta t_d, B/\Delta \nu_d, \sigma_r/\delta r_{s,iso})$. The off-source rms is $\sigma_+ = \frac{1}{2}(\Delta t B N_p)^{-1/2} \langle \mathcal{N} \rangle$ where $\Delta t = 1.12$ ms and $N_p = 112$ s = T/P , and $B = 25$ kHz. In the absence of a source, the rms visibility is $\sqrt{2}\sigma_+$. We have used the geometric mean of the off-pulse system noise for the two sites, $\langle \mathcal{N} \rangle = (\langle N_i \rangle \langle N_j \rangle)^{1/2}$, expressed in flux-density units, and the source strength I_{s0} is the flux density in the pulse-phase window used to calculate visibilities. This is much larger than the catalogued, period-averaged flux density. For Vela, the flux density at 2.5 GHz in the pulse phase window used by G97 is about 10 Jy and the intrinsic modulation index of the pulses (from activity in the neutron star magnetosphere) is about unity (Krishamohan & Downs 1983). Evidently, the flux density varies substantially on long time scales (e.g. Sieber 1973). This is not surprising given the occurrence of refractive interstellar scintillations (e.g. Kaspi & Stinebring 1992). We therefore take I_{s0} to be an unknown and consider SNR to be a variable to be fitted for.

4.1. Analysis of G97 Data

G97 report their results in arbitrary correlation units. We use the off-pulse PDF in their Figure 2 to estimate (from the mode of the PDF), $\sigma_+ \approx 550 \pm 50$ in these units. We then search over a grid in N_{ISS} and SNR to maximize the likelihood function. The expected mean flux density in the gating window can be estimated roughly from the shape of Gwinn *et al.*'s histogram and from theoretical PDFs. For the range of SNR and TB averaging relevant, the mean intensity is approximately the number of correlation units where the PDF has fallen to 50% of its peak value. From Figure 2 of Gwinn *et al.*, this is roughly 3600 to 4400 correlation units, implying $\text{SNR} \approx 7.5 \pm 0.5$. We use these coarse estimates solely to define a search grid for N_{ISS} and SNR.

Figure 3 shows (log) likelihood contours plotted against N_{ISS} and SNR. The plus sign in the figure designates the location of maximum likelihood while the vertical lines indicate ranges of N_{ISS} expected using different estimates for the DISS parameters and using either a scattering screen with a square-law structure function or a screen with Kolmogorov electron density fluctuations. The figure caption gives details. The best-fit $\text{SNR} \approx 7.6$ is consistent with our crude estimate above.

The contours indicate that N_{ISS} and SNR are anticovariant: the best fit N_{ISS} increases as SNR decreases. This occurs because, as noted by G00, the peak of the visibility histogram is the feature most sensitive to model parameters. As either N_{ISS} or SNR increases the peak moves to the right. (For example, the variation with N_{ISS} is shown in Figure 12 of Paper I.) Therefore the two quantities must compensate each other in order to match the peak and are thus negatively correlated. Based on contours that we do not show, we note that smaller values of σ_+ move the plotted likelihood contours upward and toward the right. This also is consistent with the trend just mentioned. Therefore acceptable fits are found from a family of values for SNR, N_{ISS} and σ_+ .

Another source of uncertainty results from the assumed scattering medium. The choice of medium doesn't alter the location of the contours¹ but it does alter the mapping of T , B and source size to N_{ISS} . Usage of a square-law medium rather than one with Kolmogorov statistics moves N_{ISS} to lower values.. Considering uncertainties in the type of medium relevant and in the DISS parameters, a conservative conclusion is that the maximum likelihood solution for N_{ISS} can be accounted for fully by time-bandwidth averaging without invoking any contributions from a finite source size.

The observed histogram and the PDF obtained using our best fit parameters are shown in Figure 4. The agreement of the histogram with our PDF, based on a point source and accounting for TB averaging, is as good as G97's PDF (their Figure 2), which was based on an extended source but ignored TB averaging. This shows that not only is our best fit consistent with N_{ISS} expected for a point source (and TB averaging), but also that it is as good a fit as can be expected.

We conclude that the measurements of G97 imply only an upper bound on the source size of the Vela pulsar using the DISS method. To constrain the allowed source size, we recalculate the likelihood by varying $\sigma_r/\delta r_{s,iso}$, calculating m_{ISS}^2 for a thin-screen, Kolmogorov medium while accounting for TB averaging and, hence, calculating N_{ISS} as a function of $\sigma_r/\delta r_{s,iso}$. We then use N_{ISS} to calculate, in turn, $f_G(G)$, the visibility PDF, the likelihood, and the posterior PDF for $\sigma_r/\delta r_{s,iso}$. These calculations were made by integrating over a grid of values for Δt_d , $\Delta \nu_d$, SNR, and σ_+ to take into account their uncertainties. The resultant posterior PDF and CDF for the source size are shown in Figure 5 as dashed lines. The solid lines are the PDF and CDF obtained when we fix SNR and σ_+ at their best-fit values. We use the DISS parameter values from G00 rather than from G97 because we then obtain a larger upper bound on source size. That is, we derive the least restrictive upper bound. If we use G97 parameter values and a Kolmogorov screen, the visibility fluctuations are actually quite small compared to what is predicted. If we assume a square-law screen, however, then the N_{ISS} value expected from TB averaging is again consistent; we do not believe, however, that the square-law screen is consistent with DISS observations (c.f. Figure 1 and previous discussion in text). In the PDF, the most probable source size is formally $\sigma_r/\delta r_{s,iso} \sim 0.04$ but the PDF amplitude is nearly the same for zero source size. We therefore interpret the PDF and CDF in terms of an upper bound on source size. From the CDF we find that $\sigma_r/\delta r_{s,iso} \lesssim 0.096$ at the 68% confidence level and 0.16 at 95% confidence for the case where we marginalize over all parameters. Using the *largest* of the isoplanatic scales estimated in §2, we obtain an upper limit on source size at 95% confidence of 400 km if the pulsar is at $d = 0.5$ kpc and 200 km if $d = 0.25$ kpc. Use of alternative values of the DISS parameters yield even smaller upper bounds. These upper bounds are very conservative. If we fix SNR and σ_+ at their best fit values, we get an upper bound of 150 km at the 95% confidence level.

Clearly, our results imply an upper limit that is potentially much smaller than the source size

¹The reason the contours do not change is because we have used the chi-square PDF with specified N_{ISS} to calculate the PDF of the scintillation gain, G .

estimated by G97. The difference is due to our taking into account the time-bandwidth averaging in the analysis. To show this, if we pretend that time-bandwidth averaging is negligible and repeat the calculation of the PDF for source size, we find a peak that excludes zero source size corresponding to a size determination similar to that of Gwinn *et al.*, $\sigma_r \approx 0.33\delta r_{s,iso} \approx 415$ km. This inference is, of course, erroneous.

4.2. Analysis of G00 Data

G00 present a new analysis of data on the Vela pulsar that takes into account some aspects of time-bandwidth averaging. They first fit the visibility histogram using a finite source size and correct for T-B effects only after the fact. Moreover, the scintillation time scale and bandwidth are estimated simultaneously in the fitting process, yielding values that are significantly larger than values presented in G97. Larger DISS parameters cause T-B averaging to be less important so any apparent diminution of the DISS modulation is attributable mostly to source size effects. For these reasons, the source sizes derived by G00 are only slightly less than those found in G97.

The analysis in G00 appears flawed for the following reasons. First of all, the model visibility PDF used in their fits excludes contributions from pulsar noise. In practice, this is only about a 1% error in the PDF for the first pulse gate considered by G00; but then, the PDF difference they identify between a point-source model and the data is only about 4% (G00, Figure 7). Secondly, they first fit the PDF to find the source size and then, post facto, correct the source size for time-bandwidth averaging effects. Time-bandwidth averaging is handled by calculating one-dimensional integrals (Equations 6,8 in G00) and combining them. This procedure is not mathematically correct because, as noted in §3.2, the scintillation autocovariance γ_G is not factorable.

To illustrate, consider the fact that during the 10 s averaging time, the pulsar moves approximately 1400 km given its proper motion of 140 km s^{-1} , calculated for a distance of 0.5 kpc (Bailes *et al.* 1989). This is about three times the size inferred by G00 for the emission region in the first pulse gate. By calculating only a one-dimensional temporal integral corresponding to the averaging time and a separate source-size integral, the combined effects of source size and averaging are mis-estimated. This statement follows by considering the area swept out by the emission region as it is translated spatially by the pulsar’s velocity. For a circular region of radius σ_r , the area swept out $\sim \pi\sigma_r^2(1 + 2V_{p\perp}/\pi\sigma_r)$, or about three times the area of the emission region itself. As shown in Paper I (c.f. Figures 1-6), the two-dimensional source-size integral causes the scintillation variance to decline faster than does the one-dimensional temporal integral. The product of the factors is less than the proper multiple integral, therefore *overestimating* m_{ISS}^2 and thus *underestimating* N_{ISS} .

Lastly, it is unclear exactly how the scintillation parameters are fitted for in the analysis of G00. Apparently they are solved for while also fitting the visibility histogram for the size and

flux density of a source component. This differs from the standard procedure of determining the DISS parameters using the intensity correlation function, so the systematic errors in the procedure are not known. The DISS parameters are quoted to 1.5% and 4% precisions for the scintillation bandwidth and time scale, respectively. Given the number of visibility measurements used in the histogram (Table 2 of G00) and the implied number of independent ISS samples used (Eq. 30 of Paper I), the quoted measurement error for the scintillation bandwidth seems too small. Rather, it should be comparable to the error on the DISS time scale. Moreover, the scintillation parameters are significantly larger than presented by G97. It is therefore reasonable to suspect that there are systematic errors on the DISS parameters that are not included in the quoted uncertainties.

In Figure 3 we designate the range of N_{ISS} that is consistent with the DISS parameters quoted by G00. For nominal values (26 s and 66 kHz) and assuming a point source, we obtain $N_{\text{ISS}} \approx 1.125$ when adopting a Kolmogorov screen. This value is consistent with the best fit N_{ISS} needed to account for the shape of the histogram. We therefore conclude, as before, that the data of G97 are consistent with a point source or, at least, a source whose size is below the level of detection in the scintillations.

5. Pulsar Geometries

To interpret the empirical constraints on source size that we have derived, we now turn to pulsar models and consider the physical quantities that determine source sizes.

Viable pulsar models associate most radio emission with relativistic particle flow along those magnetic field lines that extend through the velocity of light cylinder. Emission is beamed in the directions of particles' velocity vectors, which are combinations of flow along field lines and corotation velocities. In the following, we assume that beaming is predominantly tangential to the field lines, with only modest corrections from rotational aberration. The total extent of the emission region in rotational latitude and longitude is small, so corotation aberration is roughly constant over the emission region. We also assume for now that any refraction of radiation in the magnetosphere is negligible. Considerable evidence supports the view that radio emission radii are much less than r_{LC} (Rankin 1990; Cordes 1992 and references therein).

5.1. Size of the Overall Emission Region

We distinguish between the extent of the overall emission region — where all pulse components originate — from the instantaneous size responsible for emission seen at a specific pulse phase. The latter is expected to be smaller than the former because of relativistic beaming and pulsar rotation.

What do we expect for the transverse extent of the overall emission regions? Consider the

open field-line region of the pulsar to be filled with emitting material. The natural length scale is, of course, the light-cylinder radius, r_{LC} . But detailed estimates depend on relativistic beaming, the magnetic-field topology, and the radial depth and location of emission regions. CWB83 estimate the transverse separation of emission regions responsible for *different* pulse components separated by pulse phase $\Delta\eta$ to be

$$\Delta r_s = \frac{1}{3}\Delta\eta \sin \alpha_\mu r_{em}, \quad (18)$$

where α_μ is the angle between the spin and magnetic axes and r_{em} is the emission radius. Figure 2 shows schematically the locations of emission regions for two pulse components, along with the light cylinder and the isoplanatic patch. If we consider a small span of pulse phase $\Delta\eta$ in a single pulse component (as we consider here), the same equation (18) applies. This estimate assumes constant-altitude, highly-beamed emission (with essentially infinite Lorentz factor) in directions tangential to dipolar magnetic field lines.

5.2. Instantaneous Sizes of Emission Regions

To predict the transverse extent appropriate for a single pulse component, we need alternative estimates. We again consider highly-beamed radiation along tangents to dipolar magnetic field lines, modified slightly by rotational aberration. For simplicity, we assume that the magnetic axis and the line of sight are both orthogonal to the spin axis. The pulse phase η is, for given magnetic polar angle θ and radius r ,

$$\eta \approx \pm \frac{3}{2}\theta - \frac{2(r - \bar{r})}{r_{\text{LC}}}; \quad (19)$$

the second term accounts for propagation retardation and rotational aberration (Phillips 1992) which, together, introduce a time perturbation $2c^{-1}(r - \bar{r})$ (for a nonorthogonal rotator, the two would be replaced by $[1 + \sin \alpha_\mu]$). The dual signs for θ account for emission from either side of the magnetic axis, and we define a reference radius \bar{r} that may be a weak function of frequency (Blaskiewicz, Cordes & Wasserman 1991; Phillips 1992).

It is clear from Eq. 19 that different (θ, r) combinations can correspond to the same pulse phase η . Thus, a contrived emissivity distribution could produce a very narrow pulse even for a large radial depth. However, we think it more likely that the radial extent Δr_{em} and the total angular extent θ_{max} will not be related in this way and so both will contribute to the overall width of the observed pulse. In Figure 6 we show the geometry and definitions of the radial depth, Δr_{em} , and the angular width, $\theta_{\text{max}}/2$. If the radial depth Δr_{em} is the same at all $\theta \leq \theta_{\text{max}}$, then

$$\Delta\eta \approx 3\theta_{\text{max}} + 2\Delta r_{em}/r_{\text{LC}}. \quad (20)$$

We can place limits on both Δr_{em} and θ_{max} by assuming that either one can dominate the observed pulse width. For an observed pulse width $\Delta\eta/2\pi \approx 0.05$ cycles (typical of many pulsars,

including the Vela pulsar), we have the separate limits

$$\theta_{\max} \lesssim \frac{1}{3}\Delta\eta \quad (21)$$

$$\Delta r_{em} \lesssim \frac{1}{2}\Delta\eta r_{LC}. \quad (22)$$

Another contribution to the observed pulse width may come from the radiation beam width of an individual particle. If we relax our assumption of highly beamed radiation, and allow the pulse width to be determined by the relativistic beam width, then Lorentz factors

$$\gamma_p \gtrsim \frac{3}{2\Delta\eta} \quad (23)$$

are allowed.

We now wish to calculate the instantaneous source size δr_s relevant to an observation over a vanishingly small range of pulse phase. At a fixed pulse phase, the transverse extent of the emission region is $\delta r_s = 0$ as $\Delta r_{em} \rightarrow 0$ and $\gamma_p \rightarrow \infty$. Over a small range of pulse phase, the transverse extent is given by Eq. 18. For finite depth Δr_{em} , the transverse extent (again for $\gamma_p \rightarrow \infty$) is

$$\delta r_s \approx \frac{1}{2}\Delta r_{em,\perp} \approx \Delta r_{em}\langle\theta\rangle, \quad (24)$$

where $\langle\theta\rangle$ is the mean θ over those (r, θ) in Eq. 19 that satisfy $\eta = \text{constant}$. Taking θ_{\max} as an upper limit on $\langle\theta\rangle$, we obtain

$$\delta r_s \lesssim \frac{1}{2}\Delta r_{em}\theta_{\max}. \quad (25)$$

If relativistic beaming is finite, the transverse extent due to finite Lorentz factor γ_p is

$$\delta r_s \lesssim r_{em}\gamma_p^{-1}. \quad (26)$$

Expressing these results in terms of r_{LC} we have

$$\frac{\delta r_s}{r_{LC}} \approx \begin{cases} \frac{1}{2}\epsilon_{em}\theta_{\max} \left(\frac{\Delta r_{em}}{r_{em}}\right) \lesssim \frac{1}{12}(\Delta\eta)^2 & \text{finite depth} \\ \epsilon_{em}\gamma_p^{-1} \lesssim \frac{2}{3}\epsilon_{em}\Delta\eta & \text{finite Lorentz factor,} \end{cases} \quad (27)$$

where $\epsilon_{em} \equiv r_{em}/r_{LC}$ and the limits are based on Eq. 21-22.

Pulsar phenomenology suggests that $\epsilon_{em} \lesssim 0.1$ and $\Delta\eta/2\pi \lesssim 0.1$ cycles, implying nearly identical upper limits in Eq. 27 that are $\sim 3\%$ of r_{LC} . However, the true limits are probably much smaller. Rankin (1990, 1993) has shown that pulse widths (in cycles) scale $\propto P^{-1/2}$, as expected if they are determined by the angular extent of the open field-line region near the magnetic axis. (A slightly different scaling has been described by Lyne & Manchester [1988].) This implies that any contributions from relativistic beaming and radial depth are small. If so, the upper limits in Eq. 21-22 are probably a factor of ten smaller and the lower limit on γ_p in Eq. 23 is a factor of 10 larger.

5.3. Length Scales in the Vela Pulsar’s Magnetosphere

Using the pulse width (4.5 ms at 10%) and period (89 ms) of the Vela pulsar, we have $\Delta\eta/2\pi \approx 0.05$ cycles and Eq. 27 yields upper bounds on $\delta r_s/r_{LC}$ of 0.008 and $0.02(\epsilon_{em}/0.1)$ for radial depth and Lorentz-factor limits, respectively. These correspond to 34 and 89 km (for $\epsilon_{em} = 0.1$). Rankin (1990) has classified the radio pulse for the Vela pulsar as a ‘core’ component whose width is consistent with the angular size of the open field-line region expected for a dipolar field and for an emission radius $r_{em} \lesssim 2R_{NS}$, where $R_{NS} = 10$ km is the assumed neutron star radius. By contrast, Krishnamohan & Downs define four separate components in the radio emission. Thus $r_{em} \lesssim 20$ km, corresponding to $\epsilon_{em} \lesssim 10^{-2.3}$. With $\Delta r_{em} \lesssim r_{em}$, we obtain limits $\delta r_s/r_{LC} \lesssim 10^{-3.61}$ and $10^{-3.0}$, or $\delta r_s \approx 1$ and 4 km, respectively. The largest relevant transverse extent may in fact derive from the finite gating window used by G97 and G00, which is $\Delta\eta/2\pi = 0.013$ cycles, yielding

$$\delta r_s \approx \frac{1}{3}\Delta\eta r_{em} \approx 118\epsilon_{em} \text{ km.} \quad (28)$$

Simple pulsar geometries therefore suggest that the transverse scales of pulsar emission region(s) in the Vela pulsar should be less than the upper bound from the DISS observations and, in fact, may be very much less. In addition, using Eq. 23 and $\Delta\eta/2\pi \approx 0.01$ cycle for the component on the leading edge of Vela’s radio pulse (Krishnamohan & Downs 1983), a lower bound on the Lorentz factor is $\gamma_p \gtrsim 150$.

More complicated geometries may ensue if refraction within the pulsar magnetosphere is important, as has been suggested by a number of authors (Melrose 1979; Barnard & Arons 1986; Cordes & Wolszccan 1988; G97; G00). Refraction can duct wavemodes along magnetic field lines and then convert energy to propagating electromagnetic waves at some altitude that effectively could be defined as the ‘emission’ altitude. Any such ducting may alter the scalings of radio beam width with period from those expected from the Goldreich-Julian polar-cap size and in the absence of refraction. Differential refraction might cause radiation from disparate regions of the magnetosphere to reach the observer simultaneously. However, like the simple geometry considered here, if refraction is significant, one might also expect pulse widths to be much larger than observed, or at least larger than predicted from the size of the open-field-line region. That statement, along with the remarkable consistency of scaling laws for pulse widths with the Goldreich-Julian polar cap size and relatively small emission radii, suggests that refraction does not enlarge the transverse scales from which radio radiation emerges from pulsar magnetospheres.

We conclude that the magnetosphere of the Vela pulsar is likely to have radio emission regions with transverse scales too small to have been detected in the observations of Gwinn *et al.* It is also possible that they will *never* be detected using DISS or any other technique, for that matter, short of traveling to the vicinity of the pulsar.

5.4. Comparison with Gamma-ray Emission

High-energy emission from the Vela pulsar, such as the > 100 MeV pulsed gamma-rays seen with EGRET, shows a double pulse that is offset to later pulse phases from the radio pulse. Rankin (1990) classifies the radio pulse as a core component which, if similar to core emission from other pulsars, is consistent with an emission altitude close to the neutron star surface. Gamma-ray emission may be high-altitude “polar-cap” radiation that derives from the flow along open field lines originating near the magnetic polar cap (e.g. Harding & Muslimov 1998). Alternatively, it may be “outer-gap” emission from near the light cylinder whose beaming is highly affected by rotation (e.g. Romani 1996). Our conclusion that the radio emission’s transverse extent is small, at least in a narrow range of pulse phase, is consistent with both of these pictures of γ -ray emission.

6. Summary and Conclusions

In this paper we applied our superresolution methodology to the recent VLBI observations of the Vela pulsar by Gwinn *et al.* (1997, 2000) and find that the scintillation statistics may be accounted for fully by time-bandwidth averaging and a finite signal-to-noise ratio. Any contribution from extended source structure is less than an upper limit of about 400 km at the 95% confidence interval. This limit is larger than the size expected from conventional models that place radio emission well within the light cylinder of the pulsar and therefore is not restrictive on those models. Scintillation observations at frequencies lower than 2.5 GHz have better resolution — because the isoplanatic scale at the pulsar’s position scales as $\nu^{1.2}$ — and thus may be able to detect the finite source size. Recent work by Macquart *et al.* (2000) failed to find any effects of finite source size at 0.66 GHz.

Our results differ from those of Gwinn *et al.* for several reasons. We have used a more complete signal model combined with a rigorous treatment of time-bandwidth averaging and consideration of the substantial uncertainties in the measured scintillation parameters. These parameters, the diffraction time scale and bandwidth, determine the number of degrees of freedom encompassed by scintillation fluctuations when time-bandwidth averaging and source-size effects are considered. This number, in turn, has a strong influence on the shape of the visibility histogram, from which the source size is inferred or constrained. Another source of uncertainty is the nature of the scattering medium, viz. the wavenumber spectrum and phase structure function. We have found that the medium is close to being Kolmogorov in form by investigating the scaling laws of the scintillation parameters with frequency. We note also that if the shape of the visibility histogram is analyzed incorrectly, the inferred source size will have a systematic error that will scale with the isoplanatic length scale referenced to the location of the source (Eq. 2). The isoplanatic scale, $\delta r_{s,iso}$, scales with frequency approximately as $\nu^{1.2}$, so one would expect the mis-estimated source size to scale in the same way.

Our methodology can be applied to any radio source in the strong scattering regime, including compact active galactic nuclei and gamma-ray burst afterglows, though it is not clear that these sources are compact enough to show diffractive scintillations in this regime. In another paper, we will address sources of these types and we will also consider scintillations in the weak and transition scattering regimes.

I thank Z. Arzoumanian, S. Chatterjee, C. R. Gwinn, H. Lambert, T. J. W. Lazio, M. McLaughlin, and B. J. Rickett for useful discussions and H. Lambert and B. J. Rickett for making available their numerically-derived autocovariance functions for Kolmogorov media. This research was supported by NSF grant 9819931 to Cornell University and by NAIC, which is managed by Cornell University under a cooperative agreement with the NSF.

REFERENCES

- Bailes, M. *et al.* 1989, ApJ, 343, L53
- Barnard, J. J. & Arons, J. 1986, ApJ, 302, 138
- Blaskiewicz, M., Cordes, J. M. & Wasserman, I. 1991, ApJ, 370, 643
- Cha, A. N., Sembach, K. R. & Danks, A. C. 1999, ApJ, 515, L25.
- Cordes, J. M. 1986, ApJ, 311, 183
- Cordes, J. M. 1992 in *The Magnetospheric Structure and Emission Mechanisms of Radio Pulsars*, Proceedings IAU Colloq. 128, Eds. T. H. Hankins, J. M. Rankin & J. A. Gil, Zielona Góra, Poland: Pedagogical University Press, pp. 253-260
- Cordes, J. M. 2000, ApJ, submitted (Paper I).
- Cordes, J. M. & Lazio, T. J. W. 1991, ApJ, 376, 123
- Cordes, J. M., Weisberg, J. M. & Boriakoff, V. 1985, ApJ, 288, 221
- Cordes, J. M. & Rickett, B. J. 1998, ApJ, 507, 846
- Cordes, J. M. & Wolszczan, A. 1986, ApJ, 307, L27
- Desai, K. M., Gwinn, C. R. *et al.* 1992, ApJ, 393, L75
- Gwinn, C. R. *et al.* 1997, ApJ, 483, L53 (G97)
- Gwinn, C. R. *et al.* 1998, ApJ, 505, 928
- Gwinn, C. R. *et al.* 2000, ApJ, 531, 902 (G00)
- Harding, A. K. & Muslimov, A. G. 1998, ApJ, 500, 862
- Johnston, S., Nicastro, L. & Koribalski, B. 1998, MNRAS, 297, 108.
- Kaspi, V. & Stinebring, D. R. 1992, ApJ, 392, 530
- Krishnamohan, S. & Downs, G. S. 1983, ApJ, 265, 372.
- Lyne, A. G. & Manchester, R. N. 1988, MNRAS, 234, 477
- Macquart, J. -, Johnston, S., Walker, M. and Stinebring, D. 2000, ASP Conf. Ser. 202: Pulsar Astronomy - 2000 and Beyond, 215
- Melrose, D. B. 1979, Aust. J. Phys., 32, 61
- Phillips, J. A. 1992, ApJ, 385, 282.

Rankin, J. M. 1990, ApJ, 352, 247

Rankin, J. M. 1993, ApJ, 405, 285

Rickett, B. J. 1990, ARAA, 15, 479.

Romani, R. W. 1996, ApJ, 470, 469

Sieber, W. 1973, A&A, 28, 237

Thompson, A. R., Moran, J. M. & Swenson, G. W. 1991, *Interferometry and Synthesis in Radio Astronomy*, Krieger Publishing Co: Malabar, Florida

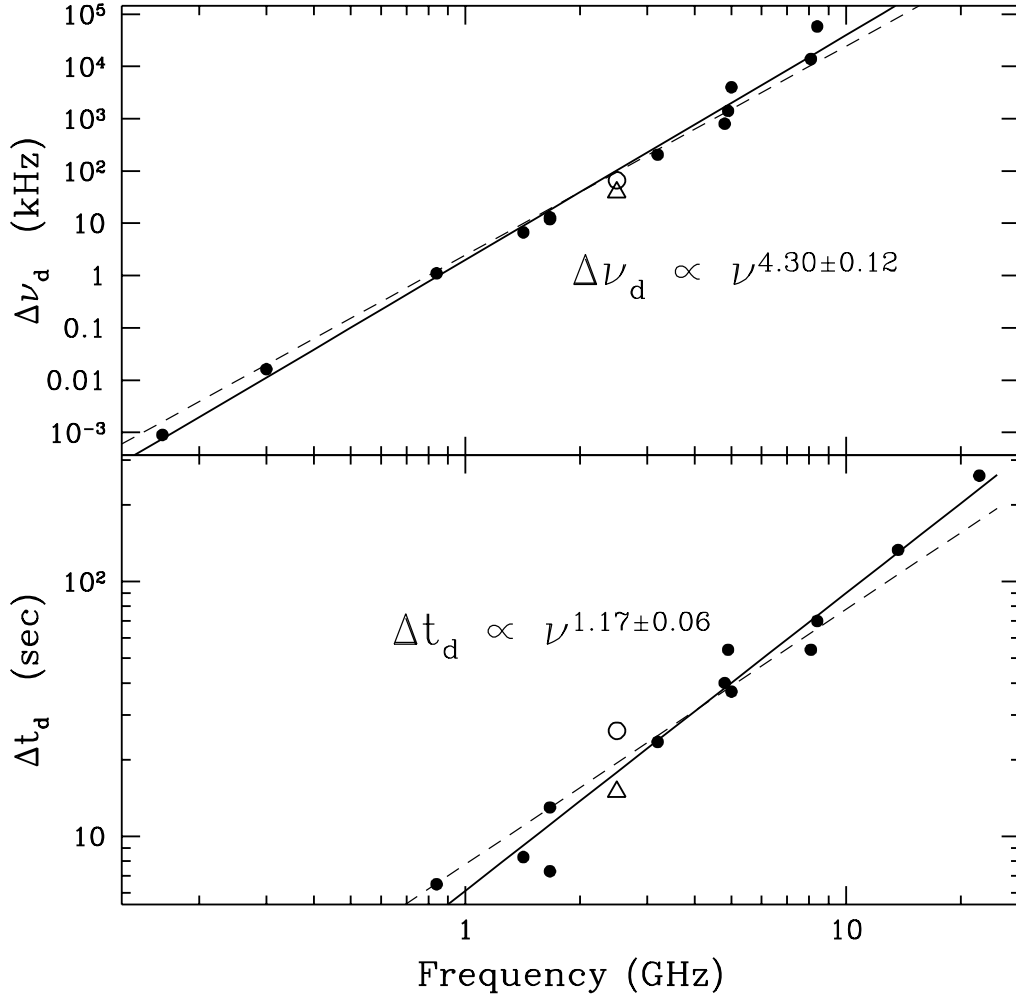


Fig. 1.— Diffractive scintillation parameters plotted against frequency. The filled circles are from Johnston *et al.* (1998) and references therein. The open triangles are from G97 and the open circles are values from G00. The solid lines are unweighted least squares fits to the filled circles of log-log quantities; errors given are $\pm 1\sigma$. The best fit scaling laws are shown. Also shown as dashed lines are the scaling laws expected for a square law structure function, i.e. $\Delta\nu_d \propto \nu^4$ and $\Delta t_d \propto \nu$. (Top Panel:) Scintillation bandwidth, $\Delta\nu_d$. The exponent is slightly smaller than the value of $22/5$ expected for a Kolmogorov medium. (Bottom Panel:) Scintillation time scale, Δt_d . The exponent is very close to that expected for a Kolmogorov medium, which is $6/5$.

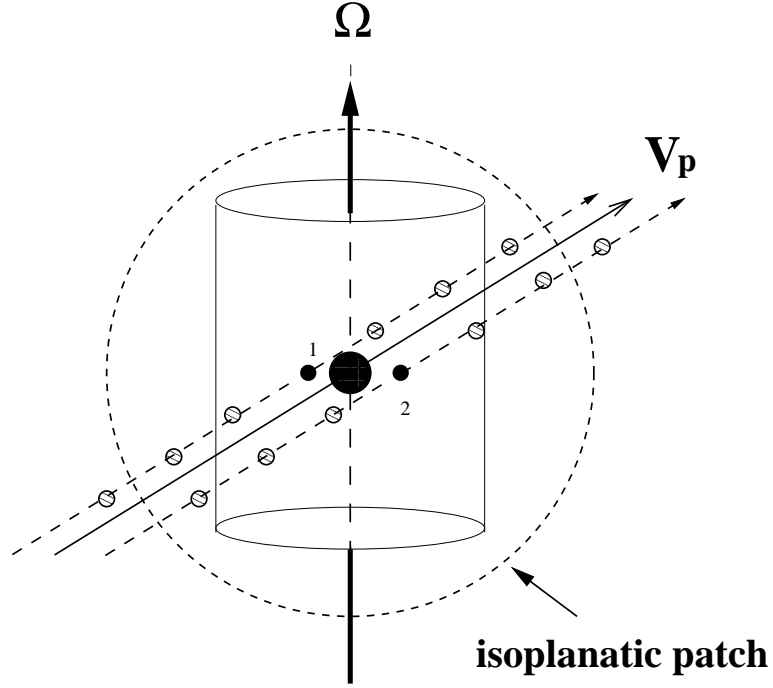


Fig. 2.— Schematic geometry for a pulsar magnetosphere, showing the light cylinder of radius c/Ω , the spin axis Ω , and the pulsar’s velocity vector, V_p . The large filled circle denotes the neutron star while the small circles labelled 1 and 2 represent the locations of emission regions at the times when radiation is beamed toward Earth to produce two pulse components. The open circles along the straight dashed lines show the locations of the emission regions as the pulsar moves translationally. The pairs of circles are separated by the distance the pulsar travels in one spin period. (Not shown is the simultaneous motion of the light cylinder.) The large dashed circle represents the isoplanatic patch size (not to scale). For many cases, the isoplanatic patch is significantly larger than the light cylinder. For the Vela pulsar, however, the patch is smaller than the light cylinder (see text).

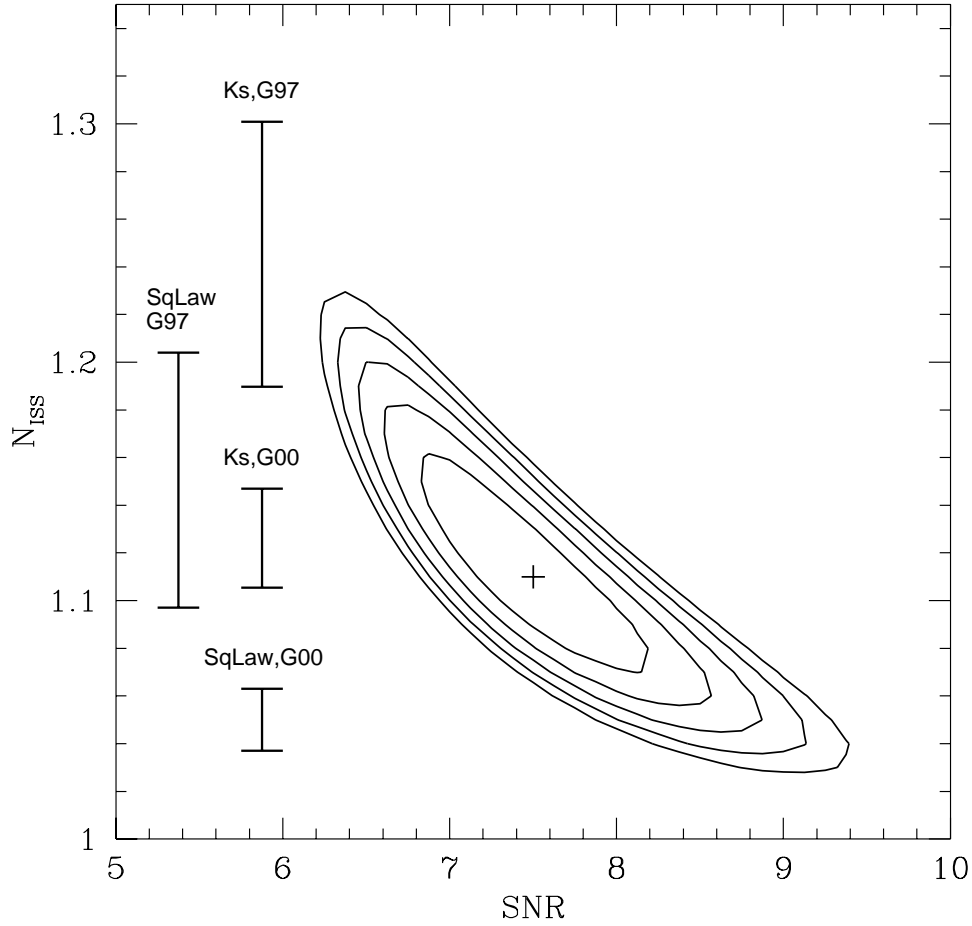


Fig. 3.— Contours of log likelihood plotted against N_{ISS} and $\text{SNR} = I_{s0}/\sqrt{2}\sigma_+$, respectively the effective number of independent DISS fluctuations in each visibility measurement and the signal to noise ratio of the pulsar flux density within the pulse-phase gate. The contours were calculated by maximizing the likelihood for the model visibility PDF given the visibility histogram of G97. The first contour is at $1/e$ from the maximum and contours are spaced at intervals $\Delta \ln \mathcal{L} = 1$. The plus sign indicates the point of maximum likelihood. The vertical lines with bars indicate ranges of N_{ISS} that correspond to different estimates (and errors) of the DISS parameters (scintillation bandwidth and time scale); the ranges are calculated by adding $\pm 1\sigma$ to each of the DISS parameters and are calculated for a point source. ‘Ks,G97’ refers to DISS parameters quoted by G97 and usage of a Kolmogorov screen to estimate N_{ISS} . ‘SqLaw,G97’ uses the same DISS parameters combined with a screen having a square-law structure function. ‘Ks,G00’ uses DISS parameters from G00 with errors estimated from our fits in Figure 1 and assuming a Kolmogorov screen. ‘SqLaw,G00’ uses a square-law screen to estimate N_{ISS} . The Kolmogorov screen is better supported by the scaling laws in Figure 1. We consider the results to signify that time-bandwidth averaging can account for the best-fit value for N_{ISS} and that the source size is consistent with being point like.

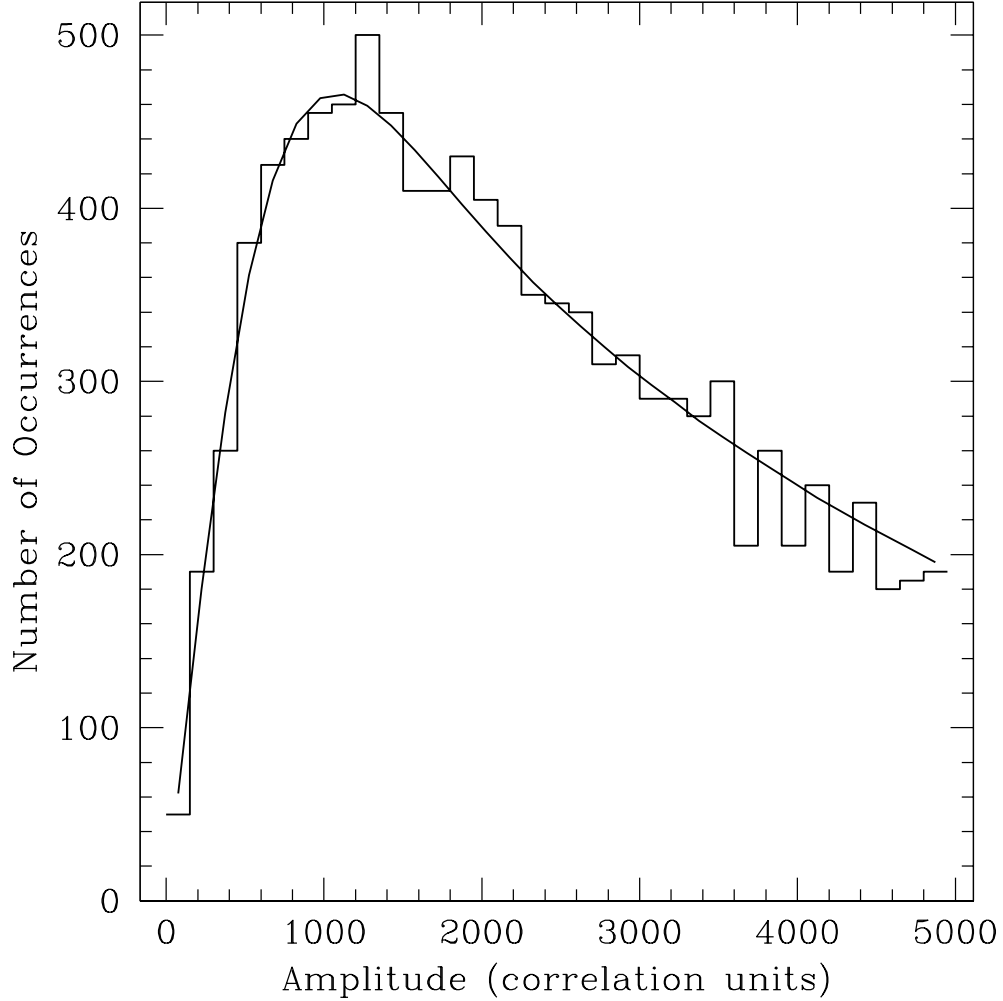


Fig. 4.— Histogram of measured visibility magnitudes from Gwinn *et al.* (1997) along with our best-fit model (smooth solid line). As implied by Figure 3, the best fit model is consistent with the source being unresolved by the DISS. That is, the value for N_{ISS} that yields the best fit to the histogram is accounted for completely by time-frequency averaging in the signal processing. A finite source size is *not* demanded by the data.

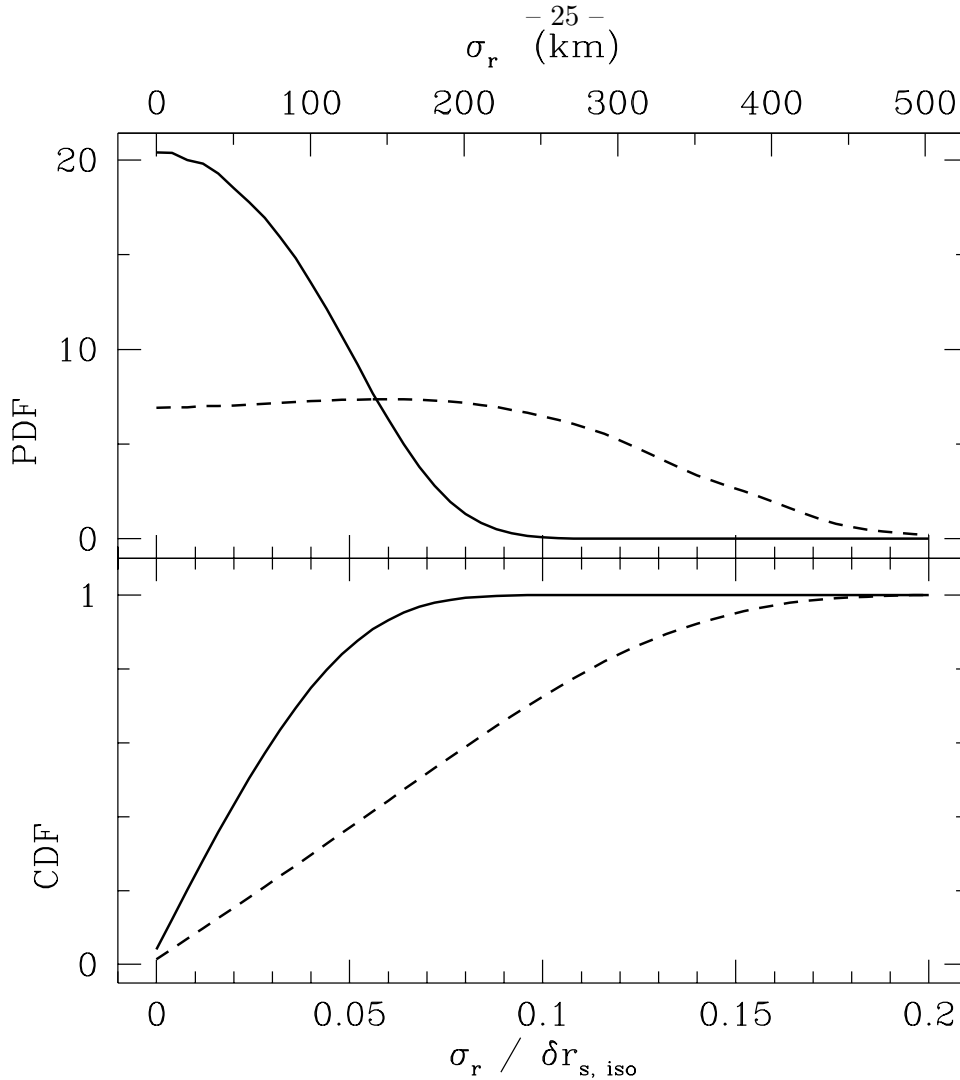


Fig. 5.— Posterior PDFs (top panel) and CDFs (bottom panel) for the source size parameter σ_r of a Gaussian brightness distribution normalized by the isoplanatic scale $\delta r_{s, iso}$ (bottom scale). The top horizontal scale expresses σ_r in kilometers, assuming a value for the isoplanatic scale of $10^{3.4}$ km. As noted in the text, the isoplanatic scale may be half this value if the pulsar is 250 pc away rather than 500 pc. The PDF was calculated by the likelihood function vs. $\sigma_r / \delta r_{s, iso}$ for fixed values of Δt_d , $\Delta \nu_d$, SNR, and σ_+ and then marginalizing over these four quantities using distributions that characterize their uncertainties. Solid lines: PDF and CDF calculated using the best fit values of SNR and σ_+ while marginalizing over distributions for the DISS parameters. Dashed lines: PDF and CDF calculated while marginalizing over distributions for SNR and σ_+ as well as for the DISS parameters.

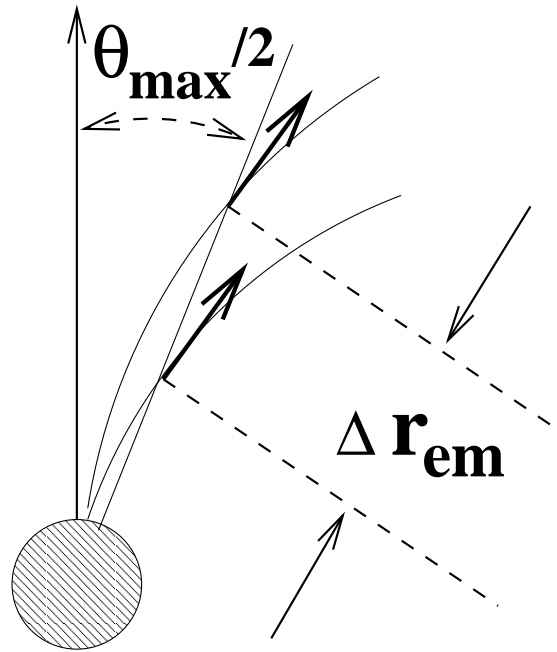


Fig. 6.— Schematic geometry for relativistic emission from the plasma flow along field lines near the magnetic pole of a radio pulsar. The total opening angle of the radiation region is θ_{\max} and the total radial depth is Δr_{em} .